Theoretical Study of the Pyrolysis of Methyltrichlorosilane in the Gas Phase. 3. Reaction Rate Constant Calculations

Yingbin Ge

Department of Chemistry, Central Washington University, Ellensburg, Washington 98926

Mark S. Gordon*

Department of Chemistry, Iowa State University, Ames, Iowa 50011

Francine Battaglia

Department of Mechanical Engineering, Virginia Polytechnic Institute and State University, Blacksburg, Virginia 24061

Rodney O. Fox

Department of Chemical and Biological Engineering, Iowa State University, Ames, Iowa 50011

Received: December 9, 2009; Revised Manuscript Received: January 6, 2010

The rate constants for the gas-phase reactions in the silicon carbide chemical vapor deposition of methyltrichlorosilane (Ge, Y. B.; Gordon, M. S.; Battaglia, F.; Fox, R. O. *J. Phys. Chem. A* **2007**, *111*, 1462.) were calculated. Transition state theory was applied to the reactions with a well-defined transition state; canonical variational transition state theory was applied to the barrierless reactions by finding the generalized transition state with the maximum Gibbs free energy along the reaction path. Geometry optimizations were carried out with second-order perturbation theory (MP2) and the cc-pVDZ basis set. The partition functions were calculated within the harmonic oscillator and rigid rotor approximations. The final potential energy surfaces were obtained using the left-eigenstate coupled-cluster theory, CR-CC(2,3) with the cc-pVTZ basis set. The high-pressure approximation was applied to the unimolecular reactions. The predicted rate constants for more than 50 reactions were compared with the experimental ones at various temperatures and pressures; the deviations are generally less than 1 order of magnitude. Theory is found to be in reasonable agreement with the experiments.

I. Introduction

Silicon carbide (SiC) is used as a protective layer in the coating of nuclear energy pellets due to its hardness, high melting point, resistance to corrosion, and imperviousness to the fission products of nuclear reactions. SiC also has the potential for replacing silicon for power devices due to its wider band gap and higher electrical breakdown field. Chemical vapor deposition (CVD) is one of the major techniques of fabricating SiC, yet the detailed gas-phase and surface chemistry of the SiC CVD are not clear.

A mechanism that consists of 114 reactions has been proposed to account for the gas-phase chemistry of the SiC CVD with methyltrichlorosilane (CH_3SiCl_3) as the precursor and H_2 as the carrier gas.[1,2] The various thermodynamic properties of ca. 50 gas-phase species[1] and ca. 70 transition states[2] have been studied theoretically using various ab initio methods. These thermodynamic properties, as well as the rate constants for the gas-phase reactions, are indispensable for carrying out kinetic simulations of the SiC CVD process. The present work aims to calculate the rate constants for *all* gas-phase reactions in the previously proposed mechanism of SiC CVD.

* Corresponding author. Tel: 515-294-0452. Fax: 515-294-5204. E-mail: mark@si.msg.chem.iastate.edu.

The rate constants for many reactions in the proposed gas-phase mechanism of SiC CVD can be found in the National Institute of Standards and Technology (NIST) chemical kinetics database[3] and in research or review articles. For example, reactions that involve small hydrocarbon molecules and radicals can be obtained from the thermodynamics and kinetics database published by Tsang and Hampson.[4] They made an attempt to thoroughly collect rate constants for all reactions related to the pyrolysis and combustion of CH_4. Their sources of the reaction rate constants include direct measurements in experiments, deduction from a complex kinetic mechanism, and theoretical calculations.[4] Tsang later compiled the rate constants for the decomposition and formation reactions of small alkanes over wide temperature and pressure ranges.[5] Baulch et al. compiled the rate constants for nearly 200 reactions, largely those related to the combustion of methane and ethane in air.[6] The experimental rate constants for most reactions of hydrocarbon species in the SiC CVD mechanism can be found in the above three articles[4–6] and the NIST chemical kinetics database.[3]

Unfortunately, fewer kinetic studies have been done for the reactions that involve chlorinated silanes; a brief introduction of such studies recorded in the NIST chemical kinetics database is given below.[3] This database fits the rate constants for each reaction into an Arrhenius-like form, $k(T) = A \cdot (T/298\ \mathrm{K})^n \cdot e^{(-E_a/RT)}$, where A is in units of s^{-1} or $cm^3\ molecule^{-1}\ s^{-1}$ for

10.1021/jp911673h
Published on Web 01/28/2010

uni- or bimolecular reactions, respectively, n is unitless, and E_a is in kJ mol^{-1}. Hereafter, only [A, n, and E_a] will be given; the large number of rate constants for various reactions at different temperatures can be obtained from the figures in the Supporting Information.

Lavrushenko, Bakianov, and Strunin studied the kinetics of the laser pyrolysis of trichlorosilane and determined the rate constant data for the reaction $SiHCl_3 \rightarrow SiCl_2 + HCl$ to be [2.51 $\times$ 10^{14}, 0, 295 $\pm$ 11.81] at 940−1070 K and 4.0 $\times$ 10^4 Pa in an argon bath.[7] Walker et al. studied the same reaction at 921 K and 1200−12900 Pa.[8] They proposed the high-pressure limit rate constant data to be [3.16 $\times$ 10^{14}, 0, 301 $\pm$ 9.06]. The above two formulas are in reasonable agreement with each other. However, the high-pressure rate constant (0.060 s^{-1}) at 1000 K calculated from the Walker formula is even lower than the rate constant (0.096 s^{-1}) measured by Lavrushenko et al. in the falloff pressure region. This implies that the accuracy of either one or both of the experiments is limited.

Doncaster and Walsh experimentally determined the rate constant expression of $Si_2Cl_6 \rightarrow SiCl_2 + SiCl_4$ to be [3.09 $\times$ 10^{13}, 0, 206 $\pm$ 2.06] at 596−655 K and 587−1173 Pa.[9] Their result is comparable to the [6.31 $\times$ 10^{13}, 0, 208] proposed by Bykovchenko, Pchelintsev, and Chernyshev who measured the rate constants for $Si_2Cl_6 \rightarrow SiCl_2 + SiCl_4$ at 633−693 K in a helium bath gas.[10]

DeSain et al. found that the rate constant for the $SiHCl_3 + Cl \rightarrow SiCl_3 + HCl$ hydrogen-abstraction reaction is pressure-independent in the ranges 296−473 K and 800−4800 Pa. Their proposed rate constant expression is [(2.3 $\pm$ 0.2) $\times$ 10^{-11}, 0, −0.55 $\pm$ 0.02].[11] The apparent activation energy is slightly negative, which indicates that this hydrogen-abstraction reaction is essentially barrierless. Serdvuk et al. measured the rate constant for the reaction $SiHCl_3 + Cl \rightarrow SiCl_3 + HCl$ to be 1.2 $\times$ 10^{-11} cm^3 molecule^{-1} s^{-1} at 298 K and 1.33 Pa in an argon bath gas.[12] For the purpose of making a direct comparison, the rate constant measured by DeSain et al. is 2.87 $\times$ 10^{-11} cm^3 molecule^{-1} s^{-1} at 298 K and 800−4800 Pa. The reasonable agreement between these two independent measurements at vastly different pressures suggests that $SiHCl_3 + Cl \rightarrow SiCl_3 + HCl$ is essentially pressure-independent.

Serdvuk et al. also studied the $SiH_2Cl_2 + Cl \rightarrow SiHCl_2 + HCl$ hydrogen-abstraction reaction and determined the reaction rate constant to be 7.01 $\times$ 10^{-11} cm^3 molecule^{-1} s^{-1} at 298 K and 1.33 Pa in an argon bath gas.[12]

Catoire, Woiki, and Roth carried out a shock tube study of the reaction $H + SiCl_4 \rightarrow HCl + SiCl_3$ at 1530−1730 K and 1.52 $\times$ 10^5 Pa.[13] They determined the forward rate constant expression of $H + SiCl_4 \rightarrow HCl + SiCl_3$ to be [(2.32 $\pm$ 0.565) $\times$ 10^{-12}, 0, 39.91 $\pm$ 21.53].

Ring, O'Neal, and Walker measured the rate constant data for the reaction $SiCl_2 + CH_4 \rightarrow CH_3SiHCl_2$ to be (2.23 $\pm$ 0.415) $\times$ 10^{-20} cm^3 molecule^{-1} s^{-1} at 921 K and 1133−12932 Pa.[14]

Kerr, Slater, and Young determined that the rate constant expression for the reaction $CH_3 + CH_3SiCl_3 \rightarrow CH_4 + CH_2SiCl_3$ is [1.26 $\times$ 10^{-11}, 0, 48.14 $\pm$ 1.45] at 378−478 K.[15] They also determined the rate constant data for $SiHCl_3 + CH_3 \rightarrow SiCl_3 + CH_4$ to be [4.37 $\times$ 10^{-11}, 0, 35.50 $\pm$ 0.36] at 303−393 K and 1867−8399 Pa.[15] Kerr, Stephens, and Young later proposed a different expression, [1.12 $\times$ 10^{-13}, 0, 17.96 $\pm$ 0.36], for the same $SiHCl_3 + CH_3 \rightarrow SiCl_3 + CH_4$ reaction, using experimental data collected at 333−443 K and 2666−4133 Pa.[16] The above three experiments were carried out in an azomethane bath gas.

Theoretical studies of the kinetics of the reactions that involve chlorinated silanes have been carried out, but these have also been limited. Walch and Dateo used computational methods to study the decomposition pathways of SiH_4, SiH_3Cl, SiH_2Cl_2, and $SiHCl_3$.[17] The optimized geometries and harmonic vibrational frequencies of the studied species were calculated at the CASSCF (complete active space self-consistent field)/cc-pVDZ level of theory. Single point CCSD(T) (coupled cluster with singles doubles and perturbative triples)/cc-pVTZ energies were also performed, and second-order perturbation theory (MP2) energies were extrapolated to the complete basis set limit.[17] Walch and Dateo further applied transition state theory (TST) to determine the rate constants at 400−1000 K. Their predicted [A, n, and E_a] are [1.5 $\times$ 10^{14}, 0, 316.3] for $SiH_2Cl_2 \rightarrow SiCl_2 + H_2$, [8.15 $\times$ 10^{-12}, 0, 169.5] for $SiCl_2 + H_2 \rightarrow SiH_2Cl_2$, [6.6 $\times$ 10^{14}, 0, 308.4] for $SiH_2Cl_2 \rightarrow SiHCl + HCl$, [3.76 $\times$ 10^{-12}, 0, 34.7] for $SiHCl + HCl \rightarrow SiH_2Cl_2$, [4.39 $\times$ 10^{14}, 0, 300.8] for $SiHCl_3 \rightarrow SiCl_2 + HCl$, and [2.52 $\times$ 10^{-12}, 0, 77.4] for $SiCl_2 + HCl \rightarrow SiHCl_3$.

Osterheld, Allendorf, and Melius applied the bond-additivity-corrected Moller−Plesset fourth-order perturbation (BAC-MP4) method to study the potential energy surface of the decomposition of CH_3SiCl_3.[18] They further calculated the high-pressure and falloff region rate constants for six decomposition reactions of CH_3SiCl_3 using Rice−Ramsperger−Kassel−Marcus (RRKM) theory and TST. Si−C bond cleavage, C−H bond cleavage, and HCl elimination reactions were found to be the predominant decomposition reactions of CH_3SiCl_3. The Si−C cleavage reaction was predicted to be faster than the C−H cleavage and HCl elimination reactions at 1300−1500 K and 10^{-3}−10^6 Torr.

Despite all the aforementioned experimental and theoretical studies, there are still many reactions in the proposed SiC CVD mechanism for which neither experimental nor theoretical rate constants are available. It is also desirable to have all of the rate constants calculated at the same level of theory, so they can be compared. The present work aims to apply transition state theory and variational transition state theory to efficiently predict the rate constants for the more than 100 gas-phase reactions in the previously proposed SiC CVD mechanism. These predicted rate constants are not expected to be highly accurate owing to the many approximations made in the calculations, which include the harmonic oscillator and rigid rotor approximations and the high-pressure approximation for the unimolecular reactions. Nevertheless, they are in reasonable agreement with experiments and can be useful in a subsequent work to perform kinetic simulations of the SiC CVD for the purpose of preliminarily reducing the current complex mechanism.[1,2]

The complete compilation of the reaction rate constants that is presented here will be used in subsequent kinetic simulations of the gas-phase chemistry of MTS that is directly relevant to the chemical vapor deposition (CVD) of silicon carbide that is very important in many processes. The comparison between the simulation results using a full gas-phase chemistry mechanism and the ones using reduced mechanisms will provide a useful guide in removing unimportant species, thereby greatly reducing the computational costs of future fluid dynamics studies of silicon carbide CVD.

II. Computational Details

The geometries of all species studied here and the transition states for the reactions of interest were optimized at the MP2/cc-pVDZ level of theory. Single point energies were obtained with coupled cluster calculations using the left-eigenstate completely renormalized (CR)-CC(2,3) method of moments

implementation, sometimes referred to with the shorthand notation CCL.[19–21] CCL/cc-pVTZ energies were estimated by assuming additivity of correlation and basis set corrections:

$$E_{\mathrm{CCL/cc\text{-}pVTZ}} \approx E_{\mathrm{CCL/cc\text{-}pVDZ}} + (E_{\mathrm{MP2/cc\text{-}pVTZ}} - E_{\mathrm{MP2/cc\text{-}pVDZ}}) \quad (1)$$

It has been shown previously that the CCL method is able to describe the bond-breaking reactions of a broad variety of C−H−Si−Cl molecules and radicals.[22,23]

Vibrational normal modes and harmonic frequencies for stationary structures were obtained through the diagonalization of the MP2/cc-pVDZ energy second derivative matrix. Partition functions were then calculated within the harmonic oscillator and rigid rotor approximations.

The rate constants for the gas-phase reactions in the SiC CVD process were calculated in the following ways:

A. Reactions with a Well-Defined Transition State. Transition state theory (TST) was used to predict the rate constants for those reactions that have a well-defined transition state. The rate constants for the unimolecular reactions were obtained using the following equation:[24]

$$k_{\mathrm{uni}} = \frac{k_{\mathrm{B}}T}{h} \mathrm{e}^{-\Delta G^{\neq 0}/k_{\mathrm{B}}T} \quad (2)$$

where k_{B} is the Boltzmann constant, T is the temperature, h is Planck's constant, and $\Delta G^{\neq 0}$ is the Gibbs energy of activation at 1 bar. The rate constants for the bimolecular reactions were calculated using a similar equation:

$$k_{\mathrm{bi}} = \frac{k_{\mathrm{B}}T}{P} \frac{k_{\mathrm{B}}T}{h} \mathrm{e}^{-\Delta G^{\neq 0}/k_{\mathrm{B}}T} \quad (3)$$

where P is the total pressure of the studied system.

Unpublished previous calculations show that TST predicted rate constants are as good as those calculated with canonical variational transition state theory (CVTST) when they are compared to experimental rate constants for reactions with energy barriers. This is because the errors in TST rate constants relative to those predicted by CVTST are often much smaller than the errors due to the harmonic oscillator and rigid rotor approximations and the errors due to the slight overestimation of energy barriers of the estimated CCL/cc-pVTZ potential energy surfaces.[22,23] For example, a 2 kcal mol^{-1} overestimation of the energy barrier will decrease the calculated rate constants by a factor of 2 at 1400 K. The treatment of a hindered rotor as a harmonic oscillator in this work may introduce even larger errors. Therefore, only TST was applied to calculate the rate constants for the reactions with a well-defined transition state.

B. Reactions without a Well-Defined Transition State. Canonical variational transition state theory (CVTST) was applied to calculate the rate constants for those reactions that do not have a well-defined transition state, such as simple bond-breaking reactions. For a barrierless reaction in which a chemical bond breaks, several nonstationary structures have been optimized at increasing bond lengths, with the breaking bond distance held fixed. The nonstationary structure with the maximum Gibbs energy along this "reaction path" was then taken to be the generalized transition state (GTS). In the diagonalization of the energy second derivative matrix at this point, the reaction mode with a nonzero gradient was projected out along with the translational and rotational modes.

Finally, tunneling effects are neglected in all of the rate constant calculations because they are of little significance at the SiC CVD temperatures (usually higher than 1400 K). For example, the small-curvature tunneling coefficient of the $SiCl_3 + H_2 \rightarrow SiHCl_3 + H$ hydrogen abstraction reaction was determined to be 1.07 (1.02) at 1400 (2000) K using the POLYRATE program.[25]

III. Results and Discussion

A. Reactions with a Transition State. Table 1 lists the forward and reverse rate constants for the 77 reactions with a transition state at 6 typical SiC CVD temperatures between 1000 and 2000 K. Because higher-level calculations have been performed in the interim, the number of species and reactions summarized in Table 1 are slightly modified from the previous work.[2] Due to the large number of studied reactions, only a subset of the TST predicted rate constants are compared with the experimental data in Figures 1−3. The remaining comparisons are made in the Supporting Information.

Figures 1−3 illustrate comparisons between TST rate constants and experimental data for three reactions of different types: the first involves only hydrocarbons, the second involves silicon chlorides, and the third involves both carbon and silicon species. The experimental data in Figures 1−3 are labeled with the squibs used in the NIST chemical kinetics database.[3] Every squib consists of the year of the original article, the first three letters of the first (and second if available) author's last name, and the page number(s) of the cited article.

Figure 1a shows that the predicted rate constants are in good agreement with the experimental data for the $C_2H_5 \rightarrow C_2H_4 + H$ unimolecular decomposition reaction. The squares are the high-pressure limit rate constants extrapolated by Dean from experimental data;[26] the triangles are the rate constants measured by Hidaka et al. in the falloff region of $(1.72-2.53) \times 10^5$ Pa.[27] The two experiments show that rate constants in the falloff pressure region are, as expected, lower than those at the high-pressure limit for the unimolecular decomposition reaction.

Figure 1b shows that the predicted rate constants for $C_2H_4 + H \rightarrow C_2H_5$ are also in good agreement with the experimental data at CVD temperatures ranging from 1000 to 2000 K. The squares and triangles are the high-pressure limit rate constants extrapolated from experimental data by Curran[28] and by Michael et al.,[29] respectively. The larger deviation of the predicted rate constants from the experimental data at lower temperatures is likely due to the omission of tunneling effects in the rate constant calculations.

Figure 2 shows that the TST rate constants for the $SiHCl_3 \rightarrow SiCl_2 + HCl$ unimolecular decomposition reaction are in good agreement with the experimental data. The squares are the high-pressure rate constants extrapolated by Walker et al. from experimental data;[8] the triangles are directly measured by Lavrushenko et al. in the falloff region at the pressure of 4.0×10^4 Pa.[7] The agreement between the two experiments suggests that the rate constant of the $SiHCl_3 \rightarrow SiCl_2 + HCl$ reaction is virtually pressure independent within a wide pressure range.

Figure 3 shows that the TST rate constants are also in good agreement with the experimental data for the $SiHCl_3 + CH_3 \rightarrow SiCl_3 + CH_4$ reaction at temperatures between 298 and 450 K. The squares are the high-pressure limit rate constants extrapolated from experimental data by Kerr, Stephens, and Young;[16] the triangles by Kerr, Slater, and Young.[15] Unfortunately, experimental rate constant data for this reaction are not available for comparison at higher temperatures.

TABLE 1: Forward (Upper Entry) and Reverse (Lower Entry) Rate Constants for the Studied Gas-Phase Reactions with a Transition State[a]

reaction	1000 K	1200 K	1400 K	1600 K	1800 K	2000 K
$CH_3SiCl_3 \rightarrow CH_2SiCl_2 + HCl$	1.3×10^{-4}	1.6×10^{-1}	2.6×10	1.2×10^{3}	2.3×10^{4}	2.5×10^{5}
	4.5×10^{-14}	8.7×10^{-14}	1.5×10^{-13}	2.4×10^{-13}	3.5×10^{-13}	5.0×10^{-13}
$CH_3SiCl_3 \rightarrow CH_3Cl + SiCl_2$	1.8×10^{-10}	2.1×10^{-6}	1.7×10^{-3}	2.6×10^{-1}	1.3×10	2.9×10^{2}
	7.5×10^{-22}	3.3×10^{-20}	5.3×10^{-19}	4.5×10^{-18}	2.5×10^{-17}	1.0×10^{-16}
$Cl + H_2 \rightarrow HCl + H$	9.6×10^{-12}	2.1×10^{-11}	3.8×10^{-11}	6.3×10^{-11}	9.4×10^{-11}	1.3×10^{-10}
	5.9×10^{-12}	1.1×10^{-11}	1.8×10^{-11}	2.6×10^{-11}	3.6×10^{-11}	4.8×10^{-11}
$Cl + HCl \rightarrow Cl_2 + H$	2.1×10^{-21}	1.6×10^{-19}	3.8×10^{-18}	4.1×10^{-17}	2.6×10^{-16}	1.2×10^{-15}
	8.4×10^{-11}	1.1×10^{-10}	1.4×10^{-10}	1.6×10^{-10}	1.9×10^{-10}	2.1×10^{-10}
$CH_3 + H_2 \rightarrow CH_4 + H$	6.1×10^{-15}	2.2×10^{-14}	6.0×10^{-14}	1.3×10^{-13}	2.6×10^{-13}	4.5×10^{-13}
	2.0×10^{-13}	8.2×10^{-13}	2.3×10^{-12}	5.2×10^{-12}	1.0×10^{-11}	1.8×10^{-11}
$CH_3 + H \rightarrow CH_2 + H_2$	5.7×10^{-14}	2.5×10^{-13}	7.3×10^{-13}	1.7×10^{-12}	3.4×10^{-12}	6.0×10^{-12}
	1.8×10^{-13}	5.0×10^{-13}	1.1×10^{-12}	2.1×10^{-12}	3.6×10^{-12}	5.8×10^{-12}
$CH_3 + CH_3 \rightarrow CH_2 + CH_4$	3.2×10^{-14}	2.0×10^{-13}	8.2×10^{-13}	2.5×10^{-12}	6.1×10^{-12}	1.3×10^{-11}
	3.4×10^{-12}	1.5×10^{-11}	4.8×10^{-11}	1.2×10^{-10}	2.6×10^{-10}	4.9×10^{-10}
$CH_3 + HCl \rightarrow CH_3Cl + H$	1.2×10^{-19}	2.4×10^{-18}	2.1×10^{-17}	1.1×10^{-16}	4.3×10^{-16}	1.3×10^{-15}
	2.6×10^{-13}	8.5×10^{-13}	2.0×10^{-12}	4.0×10^{-12}	7.0×10^{-12}	1.1×10^{-11}
$CH_3 + HCl \rightarrow CH_4 + Cl$	3.1×10^{-13}	5.4×10^{-13}	8.4×10^{-13}	1.2×10^{-12}	1.7×10^{-12}	2.3×10^{-12}
	1.7×10^{-11}	3.8×10^{-11}	7.0×10^{-11}	1.2×10^{-10}	1.8×10^{-10}	2.6×10^{-10}
$CH_3Cl + H_2 \rightarrow CH_4 + HCl$	3.8×10^{-30}	8.9×10^{-27}	2.4×10^{-24}	1.7×10^{-22}	4.7×10^{-21}	7.1×10^{-20}
	6.0×10^{-35}	9.1×10^{-31}	9.5×10^{-28}	1.8×10^{-25}	1.1×10^{-23}	3.3×10^{-22}
$CH_2Cl + HCl \rightarrow CH_2Cl_2 + H$	8.8×10^{-21}	2.3×10^{-19}	2.5×10^{-18}	1.6×10^{-17}	6.9×10^{-17}	2.3×10^{-16}
	7.9×10^{-13}	2.3×10^{-12}	5.1×10^{-12}	9.6×10^{-12}	1.6×10^{-11}	2.4×10^{-11}
$C_2H_6 \rightarrow C_2H_4 + H_2$ $(C_2)^b$	8.1×10^{-14}	3.0×10^{-9}	5.7×10^{-6}	1.7×10^{-3}	1.4×10^{-1}	4.8
	2.1×10^{-32}	5.4×10^{-29}	1.6×10^{-26}	1.1×10^{-24}	3.4×10^{-23}	5.2×10^{-22}
$C_2H_6 \rightarrow C_2H_4 + H_2$ $(C_s)^b$	5.3×10^{-12}	1.2×10^{-7}	1.5×10^{-4}	3.3×10^{-2}	2.2	6.4×10
	1.4×10^{-30}	2.1×10^{-27}	4.1×10^{-25}	2.3×10^{-23}	5.4×10^{-22}	6.9×10^{-21}
$C_2H_6 + H \rightarrow C_2H_5 + H_2$	1.2×10^{-12}	3.9×10^{-12}	9.5×10^{-12}	1.9×10^{-11}	3.3×10^{-11}	5.4×10^{-11}
	1.3×10^{-15}	5.0×10^{-15}	1.4×10^{-14}	3.1×10^{-14}	6.1×10^{-14}	1.1×10^{-13}
$C_2H_5 \rightarrow C_2H_4 + H$	3.9×10^{4}	1.1×10^{6}	1.3×10^{7}	8.3×10^{7}	3.5×10^{8}	1.1×10^{9}
	9.4×10^{-12}	1.6×10^{-11}	2.5×10^{-11}	3.5×10^{-11}	4.6×10^{-11}	5.9×10^{-11}
$C_2H_4 \rightarrow CH_2C + H_2$	1.3×10^{-6}	4.6×10^{-3}	1.6	1.3×10^{2}	4.1×10^{3}	6.4×10^{4}
	1.2×10^{-14}	3.4×10^{-14}	7.6×10^{-14}	1.4×10^{-13}	2.5×10^{-13}	3.9×10^{-13}
$CH_2C \rightarrow C_2H_2$[c]	5.5×10^{12}	6.6×10^{12}	7.6×10^{12}	8.5×10^{12}	9.2×10^{12}	9.8×10^{12}
	4.2×10^{4}	1.7×10^{6}	2.4×10^{7}	1.7×10^{8}	8.0×10^{8}	2.7×10^{9}
$C_2H_4 \rightarrow C_2H_2 + H_2$[d]	4.5×10^{-10}	4.8×10^{-6}	3.7×10^{-3}	5.5×10^{-1}	2.7×10	6.1×10^{2}
	3.3×10^{-26}	9.3×10^{-24}	5.5×10^{-22}	1.2×10^{-20}	1.4×10^{-19}	1.0×10^{-18}
$C_2H_4 + H \rightarrow C_2H_3 + H_2$	3.4×10^{-14}	1.8×10^{-13}	6.4×10^{-13}	1.7×10^{-12}	3.6×10^{-12}	6.9×10^{-12}
	4.2×10^{-14}	1.2×10^{-13}	2.7×10^{-13}	5.2×10^{-13}	9.0×10^{-13}	1.4×10^{-12}
$C_2H_3 \rightarrow C_2H_2 + H$	7.4×10^{4}	2.7×10^{6}	3.5×10^{7}	2.5×10^{8}	1.1×10^{9}	3.8×10^{9}
	4.3×10^{-12}	8.0×10^{-12}	1.3×10^{-11}	1.8×10^{-11}	2.4×10^{-11}	3.1×10^{-11}
$C_2H_3 + CH_4 \rightarrow C_2H_4 + CH_3$	8.2×10^{-15}	3.9×10^{-14}	1.3×10^{-13}	3.3×10^{-13}	7.3×10^{-13}	1.4×10^{-12}
	2.0×10^{-16}	1.6×10^{-15}	7.8×10^{-15}	2.7×10^{-14}	7.4×10^{-14}	1.7×10^{-13}
$C_2H_3 + C_2H_6 \rightarrow C_2H_4 + C_2H_5$	1.2×10^{-14}	4.5×10^{-14}	1.3×10^{-13}	3.0×10^{-13}	6.0×10^{-13}	1.1×10^{-12}
	9.9×10^{-18}	8.6×10^{-17}	4.4×10^{-16}	1.6×10^{-15}	4.4×10^{-15}	1.1×10^{-14}
$C_2H_2 + H \rightarrow C_2H + H_2$	5.8×10^{-17}	1.3×10^{-15}	1.2×10^{-14}	6.8×10^{-14}	2.6×10^{-13}	7.8×10^{-13}
	4.8×10^{-11}	8.9×10^{-11}	1.5×10^{-10}	2.2×10^{-10}	3.2×10^{-10}	4.5×10^{-10}
$C_2H_6 + CH_3 \rightarrow C_2H_5 + CH_4$	1.6×10^{-14}	9.2×10^{-14}	3.5×10^{-13}	1.0×10^{-12}	2.4×10^{-12}	5.0×10^{-12}
	5.6×10^{-16}	4.2×10^{-15}	1.9×10^{-14}	6.4×10^{-14}	1.7×10^{-13}	3.9×10^{-13}
$C_2H_6 + CH_2 \rightarrow C_2H_5 + CH_3$	1.4×10^{-13}	5.3×10^{-13}	1.5×10^{-12}	3.4×10^{-12}	6.8×10^{-12}	1.2×10^{-11}
	4.7×10^{-17}	3.3×10^{-16}	1.4×10^{-15}	4.5×10^{-15}	1.2×10^{-14}	2.6×10^{-14}
$C_2H_4 + HCl \rightarrow C_2H_5Cl$	2.3×10^{-22}	1.3×10^{-20}	2.4×10^{-19}	2.3×10^{-18}	1.4×10^{-17}	5.9×10^{-17}
	5.7	1.0×10^{3}	4.1×10^{4}	6.6×10^{5}	5.8×10^{6}	3.3×10^{7}
$C_2H_2 + HCl \rightarrow C_2H_3Cl$	8.6×10^{-23}	6.6×10^{-21}	1.6×10^{-19}	1.7×10^{-18}	1.2×10^{-17}	5.4×10^{-17}
	7.2×10^{-3}	4.6	4.8×10^{2}	1.6×10^{4}	2.4×10^{5}	2.1×10^{6}
$C_2H_5 + HCl \rightarrow C_2H_5Cl + H$	4.7×10^{-20}	7.9×10^{-19}	6.4×10^{-18}	3.2×10^{-17}	1.2×10^{-16}	3.4×10^{-16}
	2.8×10^{-13}	8.6×10^{-13}	2.0×10^{-12}	3.8×10^{-12}	6.5×10^{-12}	1.0×10^{-11}
$C_2H_5 + HCl \rightarrow C_2H_6 + Cl$	1.6×10^{-13}	2.4×10^{-13}	3.4×10^{-13}	4.6×10^{-13}	6.1×10^{-13}	7.9×10^{-13}
	2.4×10^{-10}	3.6×10^{-10}	5.1×10^{-10}	6.8×10^{-10}	8.7×10^{-10}	1.1×10^{-9}
$C_2H_3 + HCl \rightarrow C_2H_3Cl + H$	3.9×10^{-18}	4.3×10^{-17}	2.6×10^{-16}	1.0×10^{-15}	3.2×10^{-15}	8.1×10^{-15}
	1.9×10^{-14}	9.0×10^{-14}	2.8×10^{-13}	6.9×10^{-13}	1.4×10^{-12}	2.5×10^{-12}
$C_2H_3 + HCl \rightarrow C_2H_4 + Cl$	1.5×10^{-12}	2.1×10^{-12}	2.8×10^{-12}	3.6×10^{-12}	4.7×10^{-12}	5.9×10^{-12}
	2.0×10^{-12}	6.1×10^{-12}	1.4×10^{-11}	2.8×10^{-11}	4.9×10^{-11}	7.8×10^{-11}
$CH_2 + HCl \rightarrow CH_3 + Cl$	1.5×10^{-11}	2.3×10^{-11}	3.4×10^{-11}	4.7×10^{-11}	6.4×10^{-11}	8.4×10^{-11}
	7.8×10^{-12}	2.2×10^{-11}	4.9×10^{-11}	9.3×10^{-11}	1.6×10^{-10}	2.4×10^{-10}
$CH_2 + HCl \rightarrow CH_2Cl + H$	1.1×10^{-17}	1.4×10^{-16}	8.9×10^{-16}	3.8×10^{-15}	1.2×10^{-14}	3.2×10^{-14}
	1.4×10^{-14}	6.2×10^{-14}	1.9×10^{-13}	4.5×10^{-13}	9.0×10^{-13}	1.6×10^{-12}
$SiCl_2 + SiCl_4 \rightarrow Si_2Cl_6$	1.7×10^{-17}	1.1×10^{-16}	4.6×10^{-16}	1.4×10^{-15}	3.5×10^{-15}	7.6×10^{-15}
	9.0×10^{2}	4.9×10^{4}	8.5×10^{5}	7.3×10^{6}	3.9×10^{7}	1.5×10^{8}
$SiCl_4 + H_2 \rightarrow SiHCl_3 + HCl$	1.9×10^{-24}	4.6×10^{-22}	2.5×10^{-20}	5.2×10^{-19}	5.7×10^{-18}	4.0×10^{-17}
	1.5×10^{-22}	1.0×10^{-20}	2.3×10^{-19}	2.5×10^{-18}	1.7×10^{-17}	7.9×10^{-17}

TABLE 1 Continued

reaction	1000 K	1200 K	1400 K	1600 K	1800 K	2000 K
$SiCl_3 + H_2 \rightarrow SiHCl_3 + H$	1.3×10^{-15}	7.9×10^{-15}	3.0×10^{-14}	8.6×10^{-14}	2.0×10^{-13}	4.2×10^{-13}
	7.8×10^{-12}	1.5×10^{-11}	2.5×10^{-11}	3.8×10^{-11}	5.3×10^{-11}	7.2×10^{-11}
$SiCl_3 + H_2 \rightarrow SiHCl_2 + HCl$	9.1×10^{-23}	7.0×10^{-21}	1.6×10^{-19}	1.8×10^{-18}	1.2×10^{-17}	5.9×10^{-17}
	2.5×10^{-20}	5.0×10^{-19}	4.5×10^{-18}	2.4×10^{-17}	9.3×10^{-17}	2.8×10^{-16}
$SiCl_3 + HCl \rightarrow SiCl_4 + H$	1.6×10^{-16}	1.0×10^{-15}	4.2×10^{-15}	1.3×10^{-14}	3.1×10^{-14}	6.5×10^{-14}
	1.2×10^{-14}	8.7×10^{-14}	3.7×10^{-13}	1.1×10^{-12}	2.7×10^{-12}	5.6×10^{-12}
$SiCl_3 + HCl \rightarrow SiHCl_3 + Cl$	3.6×10^{-14}	1.1×10^{-13}	2.6×10^{-13}	5.3×10^{-13}	9.5×10^{-13}	1.6×10^{-12}
	3.3×10^{-10}	4.0×10^{-10}	4.7×10^{-10}	5.6×10^{-10}	6.5×10^{-10}	7.4×10^{-10}
$SiCl_2 + H_2 \rightarrow SiH_2Cl_2$	2.0×10^{-21}	7.4×10^{-20}	1.0×10^{-18}	7.9×10^{-18}	4.0×10^{-17}	1.5×10^{-16}
	5.4×10^{-3}	2.7	2.4×10^{2}	6.8×10^{3}	9.2×10^{4}	7.4×10^{5}
$SiCl_2 + H_2 \rightarrow SiHCl + HCl$	5.5×10^{-20}	1.3×10^{-18}	1.2×10^{-17}	7.2×10^{-17}	3.0×10^{-16}	9.4×10^{-16}
	1.4×10^{-14}	2.9×10^{-14}	5.2×10^{-14}	8.4×10^{-14}	1.3×10^{-13}	1.8×10^{-13}
$SiCl_2 + H_2 \rightarrow SiHCl_2 + H$	1.4×10^{-22}	1.6×10^{-20}	5.0×10^{-19}	7.0×10^{-18}	5.6×10^{-17}	3.1×10^{-16}
	5.2×10^{-10}	4.3×10^{-10}	3.9×10^{-10}	3.7×10^{-10}	3.6×10^{-10}	3.6×10^{-10}
$SiCl_2 + HCl \rightarrow SiCl_3 + H$	5.1×10^{-21}	2.1×10^{-19}	3.3×10^{-18}	2.7×10^{-17}	1.4×10^{-16}	5.7×10^{-16}
	6.6×10^{-11}	7.8×10^{-11}	9.2×10^{-11}	1.1×10^{-10}	1.2×10^{-10}	1.4×10^{-10}
$SiHCl_3 \rightarrow SiCl_2 + HCl$	2.3×10^{-1}	8.0×10	5.3×10^{3}	1.2×10^{5}	1.4×10^{6}	1.0×10^{7}
	5.0×10^{-17}	3.2×10^{-16}	1.3×10^{-15}	3.7×10^{-15}	9.1×10^{-15}	1.9×10^{-14}
$SiH_2Cl_2 \rightarrow SiHCl + HCl$	7.4×10^{-2}	3.0×10	2.2×10^{3}	5.4×10^{4}	6.7×10^{5}	5.0×10^{6}
	6.8×10^{-15}	1.8×10^{-14}	4.0×10^{-14}	7.4×10^{-14}	1.2×10^{-13}	2.0×10^{-13}
$SiHCl_3 + H_2 \rightarrow SiH_2Cl_2 + HCl$	1.5×10^{-25}	3.7×10^{-23}	2.0×10^{-21}	4.3×10^{-20}	4.7×10^{-19}	3.3×10^{-18}
	8.7×10^{-23}	5.5×10^{-21}	1.1×10^{-19}	1.1×10^{-18}	7.0×10^{-18}	3.2×10^{-17}
$SiHCl_2 + H_2 \rightarrow SiH_2Cl_2 + H$	1.3×10^{-15}	7.9×10^{-15}	3.1×10^{-14}	9.0×10^{-14}	2.1×10^{-13}	4.5×10^{-13}
	1.6×10^{-11}	3.1×10^{-11}	5.1×10^{-11}	7.7×10^{-11}	1.1×10^{-10}	1.5×10^{-10}
$SiHCl_2 + HCl \rightarrow SiHCl_3 + H$	2.5×10^{-16}	1.5×10^{-15}	5.9×10^{-15}	1.7×10^{-14}	4.2×10^{-14}	8.7×10^{-14}
	5.1×10^{-15}	4.0×10^{-14}	1.8×10^{-13}	5.7×10^{-13}	1.4×10^{-12}	3.0×10^{-12}
$SiHCl_2 + HCl \rightarrow SiH_2Cl_2 + Cl$	1.1×10^{-13}	3.2×10^{-13}	7.5×10^{-13}	1.5×10^{-12}	2.7×10^{-12}	4.4×10^{-12}
	2.1×10^{-9}	2.4×10^{-9}	2.7×10^{-9}	3.2×10^{-9}	3.6×10^{-9}	4.1×10^{-9}
$SiHCl + H_2 \rightarrow SiH_3Cl$	8.6×10^{-17}	5.2×10^{-16}	2.0×10^{-15}	5.6×10^{-15}	1.3×10^{-14}	2.7×10^{-14}
	1.4	3.0×10^{2}	1.4×10^{4}	2.6×10^{5}	2.5×10^{6}	1.6×10^{7}
$SiHCl + HCl \rightarrow SiHCl_2 + H$	1.1×10^{-17}	1.1×10^{-16}	5.8×10^{-16}	2.1×10^{-15}	6.2×10^{-15}	1.5×10^{-14}
	1.7×10^{-10}	1.3×10^{-10}	1.1×10^{-10}	9.6×10^{-11}	9.1×10^{-11}	8.9×10^{-11}
$SiCl_3 + CH_4 \rightarrow CH_3SiCl_3 + H$	1.2×10^{-21}	7.5×10^{-20}	1.6×10^{-18}	1.6×10^{-17}	1.1×10^{-16}	5.0×10^{-16}
	2.2×10^{-17}	3.4×10^{-16}	2.5×10^{-15}	1.2×10^{-14}	3.8×10^{-14}	1.0×10^{-13}
$SiCl_3 + CH_4 \rightarrow SiHCl_3 + CH_3$	5.0×10^{-15}	5.0×10^{-14}	2.8×10^{-13}	1.1×10^{-12}	3.4×10^{-12}	8.6×10^{-12}
	8.6×10^{-13}	2.6×10^{-12}	6.1×10^{-12}	1.2×10^{-11}	2.2×10^{-11}	3.7×10^{-11}
$SiCl_3 + CH_3 \rightarrow SiCl_2 + CH_3Cl$	9.4×10^{-14}	2.1×10^{-13}	4.0×10^{-13}	6.8×10^{-13}	1.1×10^{-12}	1.6×10^{-12}
	1.5×10^{-17}	2.0×10^{-16}	1.4×10^{-15}	6.2×10^{-15}	2.1×10^{-14}	5.6×10^{-14}
$SiCl_3 + CH_3 \rightarrow SiHCl_3 + CH_2$	1.2×10^{-15}	1.4×10^{-14}	8.5×10^{-14}	3.5×10^{-13}	1.1×10^{-12}	2.9×10^{-12}
	2.3×10^{-11}	5.4×10^{-11}	1.1×10^{-10}	1.9×10^{-10}	3.1×10^{-10}	4.7×10^{-10}
$SiCl_2 + CH_4 \rightarrow CH_3SiHCl_2$	1.7×10^{-27}	7.1×10^{-25}	5.6×10^{-23}	1.6×10^{-21}	2.3×10^{-20}	2.0×10^{-19}
	9.1×10^{-9}	3.6×10^{-5}	1.4×10^{-2}	1.2	3.7×10	5.9×10^{2}
$CH_2SiCl_2 + H_2 \rightarrow CH_3SiHCl_2$	3.1×10^{-19}	5.2×10^{-18}	4.1×10^{-17}	2.0×10^{-16}	7.3×10^{-16}	2.1×10^{-15}
	3.3×10^{-7}	8.0×10^{-4}	2.1×10^{-1}	1.4×10	3.6×10^{2}	4.9×10^{3}
$CH_3SiHCl_2 \rightarrow CH_2SiHCl + HCl$	1.3×10^{-4}	1.3×10^{-1}	1.8×10	7.5×10^{2}	1.4×10^{4}	1.4×10^{5}
	1.1×10^{-14}	2.6×10^{-14}	5.0×10^{-14}	8.7×10^{-14}	1.4×10^{-13}	2.1×10^{-13}
$CH_3SiCl_2 + H_2 \rightarrow CH_3SiHCl_2 + H$	1.9×10^{-15}	1.0×10^{-14}	3.9×10^{-14}	1.1×10^{-13}	2.6×10^{-13}	5.2×10^{-13}
	8.3×10^{-12}	1.6×10^{-11}	2.7×10^{-11}	4.1×10^{-11}	5.8×10^{-11}	7.8×10^{-11}
$CH_2SiCl_3 + H_2 \rightarrow CH_3SiCl_3 + H$	1.1×10^{-15}	4.1×10^{-15}	1.1×10^{-14}	2.6×10^{-14}	5.1×10^{-14}	9.0×10^{-14}
	3.3×10^{-13}	1.2×10^{-12}	3.0×10^{-12}	6.4×10^{-12}	1.2×10^{-11}	1.9×10^{-11}
$CH_3 + CH_3SiCl_3 \rightarrow CH_4 + CH_2SiCl_3$	8.9×10^{-15}	4.5×10^{-14}	1.5×10^{-13}	4.2×10^{-13}	9.4×10^{-13}	1.9×10^{-12}
	9.6×10^{-16}	5.8×10^{-15}	2.3×10^{-14}	6.7×10^{-14}	1.6×10^{-13}	3.4×10^{-13}
$CH_3 + CH_3SiCl_3 \rightarrow CH_3Cl + CH_3SiCl_2$	2.7×10^{-19}	7.8×10^{-18}	9.3×10^{-17}	6.3×10^{-16}	2.9×10^{-15}	1.0×10^{-14}
	4.5×10^{-14}	1.5×10^{-13}	3.9×10^{-13}	8.3×10^{-13}	1.6×10^{-12}	2.7×10^{-12}
$SiCl_3 + CH_3SiCl_3 \rightarrow SiHCl_3 + CH_2SiCl_3$	6.6×10^{-16}	5.2×10^{-15}	2.4×10^{-14}	8.4×10^{-14}	2.3×10^{-13}	5.3×10^{-13}
	1.2×10^{-14}	3.4×10^{-14}	7.7×10^{-14}	1.5×10^{-13}	2.6×10^{-13}	4.2×10^{-13}
$SiCl_3 + CH_3SiCl_3 \rightarrow SiCl_4 + CH_3SiCl_2$	2.0×10^{-16}	2.1×10^{-15}	1.2×10^{-14}	4.5×10^{-14}	1.3×10^{-13}	3.3×10^{-13}
	1.2×10^{-15}	9.3×10^{-15}	4.4×10^{-14}	1.5×10^{-13}	4.0×10^{-13}	9.0×10^{-13}
$H + CH_3SiCl_3 \rightarrow HCl + CH_3SiCl_2$	4.7×10^{-15}	3.7×10^{-14}	1.7×10^{-13}	5.6×10^{-13}	1.4×10^{-12}	3.0×10^{-12}
	3.7×10^{-16}	2.0×10^{-15}	7.4×10^{-15}	2.1×10^{-14}	4.7×10^{-14}	9.5×10^{-14}
$Cl + CH_3SiCl_3 \rightarrow HCl + CH_2SiCl_3$	6.0×10^{-12}	1.4×10^{-11}	2.6×10^{-11}	4.5×10^{-11}	6.9×10^{-11}	1.0×10^{-10}
	1.2×10^{-14}	2.5×10^{-14}	4.6×10^{-14}	7.5×10^{-14}	1.2×10^{-13}	1.7×10^{-13}
$CH_3SiCl_2 \rightarrow H + CH_2SiCl_2$	2.3×10^{-3}	1.3	1.3×10^{2}	4.0×10^{3}	5.9×10^{4}	5.1×10^{5}
	9.5×10^{-12}	1.3×10^{-11}	1.7×10^{-11}	2.2×10^{-11}	2.7×10^{-11}	3.2×10^{-11}
$CH_3SiCl_3 \rightarrow CH_3SiCl + Cl_2$[e]	5.2×10^{-16}	5.3×10^{-11}	2.0×10^{-7}	9.9×10^{-5}	1.2×10^{-2}	5.8×10^{-1}
	9.0×10^{-16}	2.7×10^{-15}	6.3×10^{-15}	1.2×10^{-14}	2.2×10^{-14}	3.5×10^{-14}
$CH_3SiCl + H_2 \rightarrow CH_3SiH_2Cl$	8.0×10^{-19}	7.6×10^{-18}	4.0×10^{-17}	1.5×10^{-16}	4.1×10^{-16}	9.8×10^{-16}
	2.3×10^{-2}	7.5	4.8×10^{2}	1.1×10^{4}	1.2×10^{5}	8.6×10^{5}
$CH_3SiCl + HCl \rightarrow CH_3SiHCl_2$	3.5×10^{-15}	9.0×10^{-15}	1.9×10^{-14}	3.5×10^{-14}	5.8×10^{-14}	9.0×10^{-14}
	4.6×10^{-2}	1.9×10	1.4×10^{3}	3.7×10^{4}	4.6×10^{5}	3.5×10^{6}
$SiHCl_2 \rightarrow SiCl_2 + H$	6.3×10^{4}	3.6×10^{6}	6.5×10^{7}	5.8×10^{8}	3.2×10^{9}	1.2×10^{10}

TABLE 1 Continued

reaction	1000 K	1200 K	1400 K	1600 K	1800 K	2000 K
	2.8×10^{-10}	3.7×10^{-10}	4.7×10^{-10}	5.8×10^{-10}	7.0×10^{-10}	8.2×10^{-10}
$SiHCl + HCl \rightarrow SiH_2Cl + Cl$	1.5×10^{-22}	1.2×10^{-20}	3.0×10^{-19}	3.4×10^{-18}	2.3×10^{-17}	1.1×10^{-16}
	4.0×10^{-12}	7.5×10^{-12}	1.2×10^{-11}	1.8×10^{-11}	2.5×10^{-11}	3.2×10^{-11}
$SiCl_2 + HCl \rightarrow SiHCl_2 + Cl$	2.5×10^{-25}	5.8×10^{-23}	3.0×10^{-21}	6.1×10^{-20}	6.5×10^{-19}	4.5×10^{-18}
	1.5×10^{-12}	3.0×10^{-12}	5.0×10^{-12}	7.7×10^{-12}	1.1×10^{-11}	1.5×10^{-11}
$C_2H_2 + H_2 \rightarrow C_2H_3 + H$	2.4×10^{-27}	1.4×10^{-24}	1.4×10^{-22}	4.6×10^{-21}	7.0×10^{-20}	6.3×10^{-19}
	6.6×10^{-13}	1.3×10^{-12}	2.2×10^{-12}	3.4×10^{-12}	4.7×10^{-12}	6.2×10^{-12}
$C_2H_4 + H_2 \rightarrow C_2H_5 + H$	1.0×10^{-26}	6.6×10^{-24}	7.2×10^{-22}	2.6×10^{-20}	4.3×10^{-19}	4.2×10^{-18}
	6.7×10^{-13}	1.3×10^{-12}	2.2×10^{-12}	3.3×10^{-12}	4.6×10^{-12}	6.1×10^{-12}
$C_2H_4 + C_2H_4 \rightarrow C_2H_3 + C_2H_5$	9.4×10^{-28}	1.1×10^{-24}	2.0×10^{-22}	1.0×10^{-20}	2.2×10^{-19}	2.7×10^{-18}
	7.7×10^{-14}	1.5×10^{-13}	2.5×10^{-13}	3.9×10^{-13}	5.9×10^{-13}	8.4×10^{-13}
$C_2H_2 + C_2H_6 \rightarrow C_2H_3 + C_2H_5$	1.3×10^{-25}	6.5×10^{-23}	5.9×10^{-21}	1.8×10^{-19}	2.7×10^{-18}	2.5×10^{-17}
	3.8×10^{-14}	7.6×10^{-14}	1.4×10^{-13}	2.2×10^{-13}	3.4×10^{-13}	4.9×10^{-13}

[a] The units are s^{-1} or cm^3 $molecule^{-1}$ s^{-1} for the uni- or bimolecular reactions, respectively. All energy calculations were carried out at the CCL/cc-pVTZ level (eq 1); partition functions at the MP2/cc-pVDZ level. [b] $C_2H_6 \rightarrow C_2H_4 + H_2$ (C_2) is an elementary reaction pathway with C_2 point group symmetry. $C_2H_6 \rightarrow C_2H_4 + H_2$ (C_s) was previously listed as a two-step reaction:[2] $C_2H_6 \rightarrow C_2H_6$ (e) $\rightarrow C_2H_4 + H_2$; the C_2H_6 (e) $\rightarrow C_2H_4 + H_2$ reaction pathway adopts C_s symmetry, where C_2H_6 (e) is ethane with an eclipsed conformation.[2] C_2H_6 (e) has one imaginary frequency and hence is removed from the species list. [c] This was presented as a two-step reaction, $CH_2C \rightarrow HCHC \rightarrow C_2H_2$, in the previous work.[2] HCHC is an artificial intermediate structure at the MP2 level of theory and hence is removed from the species list. [d] This was presented as a two-step reaction, $C_2H_4 \rightarrow CH_3CH(s) \rightarrow C_2H_2 + H_2$, in the previous work.[2] $CH_3CH(s)$ is ethylidene with a staggered conformation. $CH_3CH(s)$ has one imaginary frequency and hence is removed from the species list. [e] This was presented as a two-step reaction, $CH_3SiCl_3 \rightarrow CH_3SiCl_2Cl \rightarrow CH_3SiCl + Cl_2$, in the previous work.[2] CH_3SiCl_2Cl is an artificial intermediate structure at the MP2 level of theory and hence is removed from the species list.

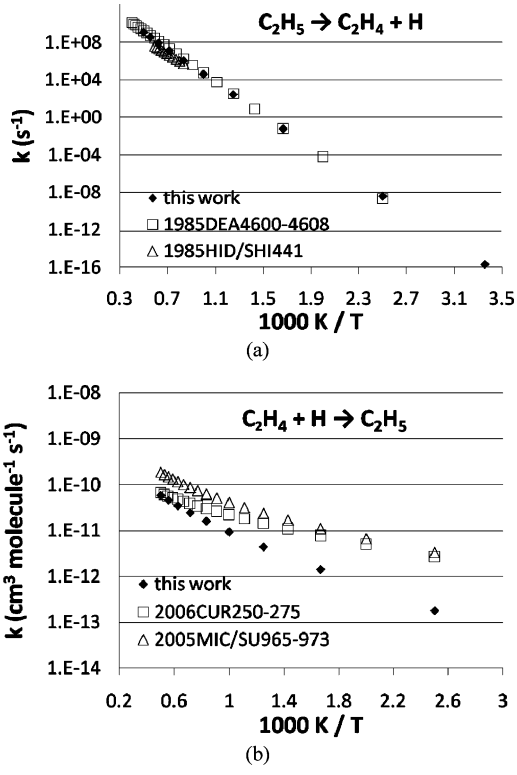

Figure 1. $C_2H_5 \rightarrow C_2H_4 + H$ bond-breaking reaction: comparison between the TST-predicted and experimental (a) forward[26,27] and (b) reverse[28,29] reaction rate constants as a function of temperature.

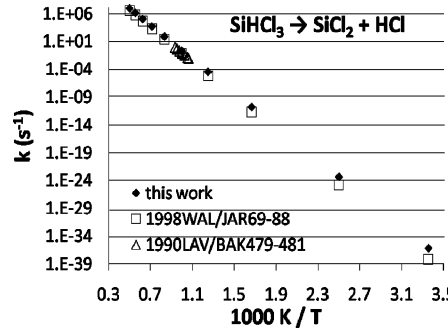

Figure 2. $SiHCl_3 \rightarrow SiCl_2 + HCl$ 1,1-HCl elimination reaction: comparison between the TST predicted and experimental forward reaction rate constants as a function of temperature.[7,8]

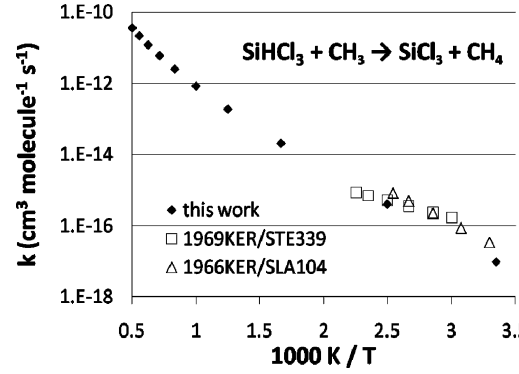

Figure 3. $SiHCl_3 + CH_3 \rightarrow SiCl_3 + CH_4$ hydrogen-abstraction reaction: comparison between the TST predicted and experimental forward reaction rate constants as a function of temperature.[15,16]

B. Reactions without a Well-Defined Transition State. The CVTST rate constants for the 27 reactions without a well-defined transition state are given in Table 2. Because the kinetic studies of these 27 reactions were done in a similar fashion, only the rate constant calculation for the $CH_4 \rightarrow CH_3 + H$ reaction is discussed in detail below.

Figure 4a shows the Gibbs energy curve of the $CH_4 \rightarrow CH_3 + H$ dissociation reaction at 1000−2000 K; Figure 4b presents the amplified data at selected C−H bond distances for a clearer view. The generalized transition state (GTS) of the $CH_4 \rightarrow CH_3 + H$ reaction has a C−H bond distance of ~3.0 Å at 1400−2000 K. The GTS has a looser structure at lower temperatures, because entropy plays a less important role and thus the potential energy is the preeminent factor in finding the GTS at low temperatures. Unfortunately, the single reference MP2 method breaks down at C−H bond distances longer than 3.2 Å. Consequently, one cannot obtain the second derivative matrix (Hessian). The CR-CC(2,3) method is stable at these distances, but this method is too expensive to use to calculate the Hessians.

TABLE 2: Forward (Upper Entry) and Reverse (Lower Entry) Rate Constants for the Studied Gas-Phase Reactions without a Transition State[a]

reaction	1000 K	1200 K	1400 K	1600 K	1800 K	2000 K
$CH_3SiCl_3 \rightarrow CH_3 + SiCl_3$	3.5×10^{-5}	7.5×10^{-2}	1.8×10	1.1×10^{3}	2.5×10^{4}	3.2×10^{5}
	9.2×10^{-13}	1.2×10^{-12}	1.7×10^{-12}	2.0×10^{-12}	2.5×10^{-12}	3.1×10^{-12}
$CH_3SiCl_3 \rightarrow CH_2SiCl_3 + H$	5.1×10^{-8}	2.8×10^{-4}	1.4×10^{-1}	1.4×10	5.2×10^{2}	9.2×10^{3}
	2.7×10^{-12}	2.8×10^{-12}	2.9×10^{-12}	3.1×10^{-12}	3.2×10^{-12}	3.4×10^{-12}
$CH_3SiCl_3 \rightarrow CH_3SiCl_2 + Cl$	8.7×10^{-8}	4.3×10^{-4}	1.9×10^{-1}	1.8×10	6.2×10^{2}	1.1×10^{4}
	1.8×10^{-10}	1.3×10^{-10}	9.9×10^{-11}	8.5×10^{-11}	7.7×10^{-11}	7.3×10^{-11}
$CH_3SiCl_3 \rightarrow CHSiCl_3 + H_2$	1.2×10^{-11}	2.6×10^{-7}	3.1×10^{-4}	6.0×10^{-2}	3.6	9.7×10
	2.3×10^{-11}	2.0×10^{-11}	1.8×10^{-11}	1.7×10^{-11}	1.6×10^{-11}	1.6×10^{-11}
$H_2 \rightarrow H + H$	3.9×10^{-8}	2.1×10^{-4}	9.8×10^{-2}	1.0×10	3.7×10^{2}	6.7×10^{3}
	6.3×10^{-10}	5.8×10^{-10}	5.5×10^{-10}	5.3×10^{-10}	5.2×10^{-10}	5.2×10^{-10}
$HCl \rightarrow H + Cl$	1.6×10^{-7}	5.9×10^{-4}	2.1×10^{-1}	1.7×10	5.2×10^{2}	8.2×10^{3}
	4.3×10^{-9}	3.1×10^{-9}	2.5×10^{-9}	2.2×10^{-9}	1.9×10^{-9}	1.8×10^{-9}
$Cl_2 \rightarrow Cl + Cl$	5.7×10	6.0×10^{3}	1.6×10^{5}	2.0×10^{6}	1.4×10^{7}	6.3×10^{7}
	3.8×10^{-11}	4.8×10^{-11}	5.6×10^{-11}	6.3×10^{-11}	7.0×10^{-11}	7.6×10^{-11}
$CH_4 \rightarrow CH_3 + H$	2.5×10^{-7}	1.7×10^{-3}	9.6×10^{-1}	1.1×10^{2}	4.2×10^{3}	7.8×10^{4}
	1.2×10^{-10}	1.3×10^{-10}	1.4×10^{-10}	1.5×10^{-10}	1.5×10^{-10}	1.6×10^{-10}
$C_2H_6 \rightarrow CH_3 + CH_3$	3.9×10^{-2}	5.9×10	9.8×10^{3}	4.6×10^{5}	8.6×10^{6}	8.8×10^{7}
	7.9×10^{-11}	7.7×10^{-11}	7.2×10^{-11}	7.2×10^{-11}	6.9×10^{-11}	6.9×10^{-11}
$CH_3 \rightarrow CH_2 + H$	2.6×10^{-8}	2.8×10^{-4}	2.1×10^{-1}	3.0×10	1.4×10^{3}	3.1×10^{4}
	1.3×10^{-9}	1.6×10^{-9}	1.8×10^{-9}	1.9×10^{-9}	2.1×10^{-9}	2.3×10^{-9}
$C_2H_5 \rightarrow CH_2 + CH_3$	9.4×10^{-7}	5.4×10^{-3}	2.7	2.8×10^{2}	1.1×10^{4}	2.0×10^{5}
	5.7×10^{-12}	1.2×10^{-11}	2.0×10^{-11}	3.3×10^{-11}	5.0×10^{-11}	7.2×10^{-11}
$C_2H_6 \rightarrow C_2H_5 + H$	4.6×10^{-7}	2.6×10^{-3}	1.3	1.4×10^{2}	5.2×10^{3}	9.3×10^{4}
	7.7×10^{-12}	9.1×10^{-12}	1.1×10^{-11}	1.2×10^{-11}	1.3×10^{-11}	1.5×10^{-11}
$C_2H_4 \rightarrow C_2H_3 + H$	7.8×10^{-9}	7.8×10^{-5}	5.8×10^{-2}	8.4	4.1×10^{2}	9.1×10^{3}
	1.5×10^{-10}	1.4×10^{-10}	1.4×10^{-10}	1.4×10^{-10}	1.4×10^{-10}	1.5×10^{-10}
$SiCl_2 + SiCl_4 \rightarrow SiCl_3 + SiCl_3$	3.6×10^{-22}	2.4×10^{-20}	4.9×10^{-19}	5.1×10^{-18}	3.3×10^{-17}	1.5×10^{-16}
	6.4×10^{-14}	1.0×10^{-13}	1.6×10^{-13}	2.3×10^{-13}	3.2×10^{-13}	4.3×10^{-13}
$Si_2Cl_5 \rightarrow SiCl_2 + SiCl_3$	1.0×10^{9}	9.5×10^{9}	4.7×10^{10}	1.5×10^{11}	3.9×10^{11}	8.3×10^{11}
	7.1×10^{-11}	6.9×10^{-11}	7.3×10^{-11}	8.1×10^{-11}	9.1×10^{-11}	1.0×10^{-10}
$Si_2Cl_4 \rightarrow SiCl_2 + SiCl_2$	9.1×10^{12}	1.5×10^{13}	2.1×10^{13}	2.2×10^{13}	2.2×10^{13}	2.2×10^{13}
	8.4×10^{-12}	8.6×10^{-12}	9.0×10^{-12}	8.1×10^{-12}	7.5×10^{-12}	7.3×10^{-12}
$Si_2Cl_6 \rightarrow SiCl_3 + SiCl_3$	1.6	7.7×10^{2}	6.2×10^{4}	1.6×10^{6}	2.0×10^{7}	1.5×10^{8}
	5.3×10^{-12}	7.8×10^{-12}	1.1×10^{-11}	1.4×10^{-11}	1.7×10^{-11}	2.2×10^{-11}
$SiCl_3 \rightarrow SiCl_2 + Cl$	1.1×10	1.9×10^{3}	7.4×10^{4}	1.2×10^{6}	9.8×10^{6}	5.4×10^{7}
	2.2×10^{-11}	2.7×10^{-11}	3.2×10^{-11}	3.7×10^{-11}	4.3×10^{-11}	4.9×10^{-11}
$SiCl_4 \rightarrow SiCl_3 + Cl$	6.0×10^{-8}	3.3×10^{-4}	1.5×10^{-1}	1.5×10	5.5×10^{2}	9.8×10^{3}
	2.1×10^{-11}	2.1×10^{-11}	2.1×10^{-11}	2.2×10^{-11}	2.3×10^{-11}	2.5×10^{-11}
$SiHCl_3 \rightarrow SiCl_3 + H$	6.9×10^{-6}	1.5×10^{-2}	3.7	2.3×10^{2}	5.4×10^{3}	7.0×10^{4}
	1.9×10^{-11}	2.2×10^{-11}	2.5×10^{-11}	2.8×10^{-11}	3.0×10^{-11}	3.2×10^{-11}
$SiHCl_3 \rightarrow SiHCl_2 + Cl$	4.2×10^{-8}	2.3×10^{-4}	1.1×10^{-1}	1.1×10	3.8×10^{2}	6.8×10^{3}
	5.4×10^{-11}	4.6×10^{-11}	4.3×10^{-11}	4.1×10^{-11}	4.1×10^{-11}	4.2×10^{-11}
$SiH_2Cl_2 \rightarrow SiH_2Cl + Cl$	3.9×10^{-8}	2.0×10^{-4}	9.2×10^{-2}	9.1	3.2×10^{2}	5.6×10^{3}
	9.3×10^{-11}	7.6×10^{-11}	6.9×10^{-11}	6.5×10^{-11}	6.4×10^{-11}	6.3×10^{-11}
$SiH_2Cl_2 \rightarrow SiHCl_2 + H$	1.9×10^{-5}	4.0×10^{-2}	9.5	5.7×10^{2}	1.4×10^{4}	1.7×10^{5}
	2.6×10^{-11}	2.9×10^{-11}	3.2×10^{-11}	3.5×10^{-11}	3.8×10^{-11}	4.0×10^{-11}
$SiCl_2 + CH_4 \rightarrow SiHCl_2 + CH_3$	3.1×10^{-24}	5.3×10^{-22}	2.2×10^{-20}	3.9×10^{-19}	3.7×10^{-18}	2.3×10^{-17}
	3.4×10^{-13}	3.8×10^{-13}	4.4×10^{-13}	5.2×10^{-13}	6.0×10^{-13}	6.9×10^{-13}
$CH_2SiCl_3 \rightarrow CH_2 + SiCl_3$	5.6×10^{-8}	4.4×10^{-4}	2.7×10^{-1}	3.4×10	1.4×10^{3}	2.9×10^{4}
	1.4×10^{-12}	4.3×10^{-12}	9.9×10^{-12}	2.0×10^{-11}	3.5×10^{-11}	5.7×10^{-11}
$CH_2SiCl_3 \rightarrow CH_2SiCl_2 + Cl$	6.9×10^{-4}	3.5×10^{-1}	3.0×10	8.2×10^{2}	1.0×10^{4}	7.7×10^{4}
	1.2×10^{-10}	1.1×10^{-10}	1.0×10^{-10}	9.9×10^{-11}	9.4×10^{-11}	9.2×10^{-11}
$CH_3SiCl_2 \rightarrow CH_3 + SiCl_2$	4.5×10^{6}	1.5×10^{8}	1.8×10^{9}	1.0×10^{10}	3.5×10^{10}	9.4×10^{10}
	1.2×10^{-10}	1.2×10^{-10}	1.4×10^{-10}	1.4×10^{-10}	1.2×10^{-10}	1.2×10^{-10}

[a] The units are s^{-1} or cm^3 molecule^{-1} s^{-1} for the uni-or bimolecular reactions, respectively. All energy calculations were carried out at the CCL/cc-pVTZ level (eq 1); partition functions at the MP2/cc-pVDZ level.

Therefore, the GTS for the $CH_4 \rightarrow CH_3 + H$ reaction at lower temperatures was taken to have a 3.2 Å C−H bond distance. This approximation underestimates the Gibbs free energy barrier and thus leads to an overestimation of the rate constants for the $CH_4 \rightarrow CH_3 + H$ reaction at temperatures lower than 1200 K. Similar approximations were made in the rate constant calculations for all other bond-breaking reactions. The errors introduced by these approximations are usually less than 1 order of magnitude; they tend to cancel the errors due to the overestimation of the energy barriers for bond breaking reactions by the CCL method.

Figure 5a shows that the CVTST predicted high-pressure limit rate constants for the $CH_4 \rightarrow CH_3 + H$ reaction at 1000−2000 K are in good agreement with the experimental results obtained by Sutherland et al.[30] and by Arutyunov et al.[31] The Sutherland et al. data are high-pressure limit rate constants extrapolated from experimental data.[30] The Arutyunov et al. data are measured at $(1.48-9.33) \times 10^4$ Pa.[31] The high-pressure limit experimental rate constants are slightly larger than the falloff region data; CVTST predicted rate constants are in better agreement with the former experiment.

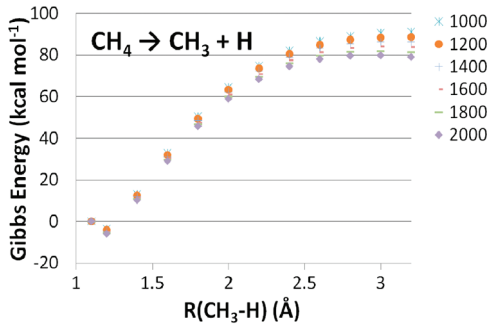

(a)

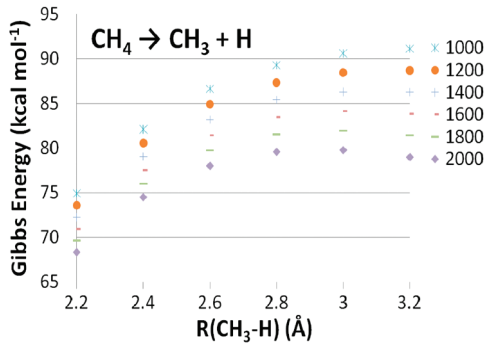

(b)

Figure 4. (a) Gibbs energy surface of the $CH_4 \rightarrow CH_3 + H$ reaction at 1000−2000 K. (b) Amplified Gibbs energy data at selected C−H bond distances.

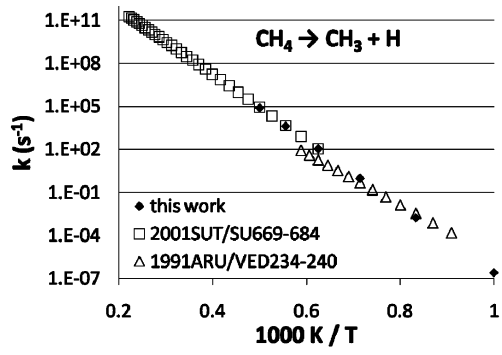

(a)

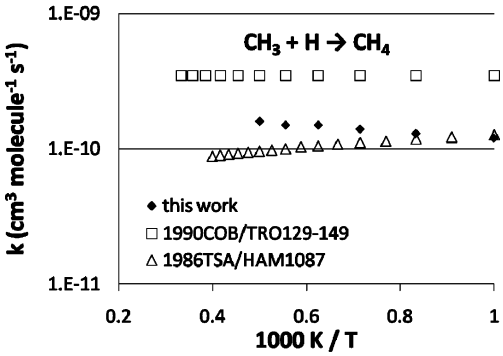

(b)

Figure 5. $CH_4 \rightarrow CH_3 + H$ bond-breaking reaction: comparison between the CVTST-predicted and experimental (a) forward[30,31] and (b) reverse[4,32] reaction rate constants.

Figure 5b shows that the CVTST rate constants for the $CH_3 + H \rightarrow CH_4$ reaction also compare satisfactorily with the experimental data.[4,32] Tsang and Hampson estimated the high-pressure limit rate constants through extensive literature review of experimental data.[4] Cobos and Troy's data are derived from fitting to a complex mechanism at 300−3000 K and 1.31×10^5 Pa in an argon bath.[32] Note that the falloff region rate constants are unexpectedly higher than the high-pressure limit data, which might indicate limitations of the experimental data, especially those for the radical recombination reactions.

The comparisons between the predicted reaction rate constants for the remaining barrierless reactions and the corresponding experimental data are presented in the Supporting Information. The predicted rate constants for all of the unimolecular reactions studied in the present work are high-pressure limit estimates. Nonetheless, most of them are reasonably close to the experimental data obtained at atmospheric pressure, and thus can be used (with caution) in future kinetic studies of SiC CVD simulations. However, for the association reaction of two *atomic* radicals, such as $H + H \rightarrow H_2$, the high-pressure limit rate constants differ significantly from the experimental data at atmospheric pressure. This is because diatomic molecules have only one vibrational mode, and thus the energized diatomic molecules formed by the association of two atomic radicals will decompose immediately unless the extra energy can be transferred through collisions. Therefore, the rate constant expression for the association reaction of two atomic radicals is proportional to the effective collision frequency, which linearly depends on the pressure.

IV. Conclusions

The rate constants for the gas-phase reactions in the previously proposed SiC CVD mechanism[1,2] were calculated using transition state theory and canonical variational transition state theory. Despite the harmonic oscillator and rigid rotor approximations made in the calculations, the TST and CVTST predicted rate constants for the bimolecular reactions agree reasonably well with the experimental data. The calculated high-pressure limit rate constants for the unimolecular decomposition reactions are also comparable to the experimental data collected at atmospheric pressure, except for the dissociation reactions of diatomic molecules and their reverse reactions. The reaction rate constants predicted in this work complement the current compilations of theoretical and experimental data for the reactions that involve C−H−Si−Cl species. The complete compilation of the reaction rate constants presented here will be used in subsequent kinetic simulations of the gas-phase chemistry of MTS that is directly relevant to the chemical vapor deposition (CVD) of silicon carbide that is very important in many processes, including the surface deposition in nuclear reactors.[33,34] These kinetic simulations will illustrate the evolving concentrations of the gas-phase species with time in the SiC CVD process. The comparison between the simulation results using a full gas-phase chemistry mechanism and the ones using reduced mechanisms will provide a useful guide in removing unimportant species, thereby greatly reducing the computational costs of future fluid dynamics studies of silicon carbide CVD.

Acknowledgment. This project was supported by the U.S. Department of Energy, Grant No. DE-FC07-05ID14661. Computer time was provided by the Scalable Computing Laboratory, Iowa State University.

Supporting Information Available: Extensive comparisons between the (canonical variational) transitions state theory predicted reaction rate constants and the experimental ones. This material is available free of charge via the Internet at http://pubs.acs.org.

References and Notes

(1) Ge, Y. B.; Gordon, M. S.; Battaglia, F.; Fox, R. O. *J. Phys. Chem. A* **2007**, *111*, 1462.
(2) Ge, Y. B.; Gordon, M. S.; Battaglia, F.; Fox, R. O. *J. Phys. Chem. A* **2007**, *111*, 1475.
(3) http://kinetics.nist.gov/kinetics/index.jsp, August, 2009.
(4) Tsang, W.; Hampson, R. F. *J. Phys. Chem. Ref. Data* **1986**, *15*, 1087.
(5) Tsang, W. *Combust. Flame* **1989**, *78*, 71.
(6) Baulch, D. L.; Cobos, C. J.; Cox, R. A.; Frank, P.; Hayman, G.; Just, T.; Kerr, J. A.; Murrells, T.; Pilling, M. J.; Troe, J.; Walker, R. W.; Warnatz, J. *J. Phys. Chem. Ref. Data* **1994**, *23*, 847.
(7) Lavrushenko, B. B.; Bakianov, A. V.; Strunin, V. P. *Spectrochim. Acta Part a-Mol. Biomol. Spectrosc.* **1990**, *46*, 479.
(8) Walker, K. L.; Jardine, R. E.; Ring, M. A.; O'Neal, H. E. *Int. J. Chem. Kinet.* **1998**, *30*, 69.
(9) Doncaster, A. M.; Walsh, R. *J. Chem. Soc., Faraday Trans. I* **1980**, *76*, 272.
(10) Bykovchenko, V. G.; Pchelintsev, V. I.; Chernyshev, E. A. *Kinet. Catal.* **1975**, *16*, 204.
(11) DeSain, J. D.; Valachovic, L.; Jusinski, L. E.; Taatjes, C. A. *J. Chem. Phys.* **2006**, *125*, 224308.
(12) Serdvuk, N. K.; Strunin, V. P.; Chesnokov, E. N.; Panfilov, V. N. *Khim. Fiz.* **1983**, 1527.
(13) Catoire, L.; Woiki, D.; Roth, P. *Int. J. Chem. Kinet.* **1997**, *29*, 469.
(14) Ring, M. A.; O'Neal, H. E.; Walker, K. L. *Int. J. Chem. Kinet.* **1998**, *30*, 89.
(15) Kerr, J. A.; Slater, D. H.; Young, J. C. *J. Chem. Soc. A* **1966**, 104.
(16) Kerr, J. A.; Stephens, A; Young, J. C. *Int. J. Chem. Kinet.* **1969**, *1*, 339.
(17) Walch, S. P.; Dateo, C. E. *J. Phys. Chem. A* **2001**, *105*, 2015.
(18) Osterheld, T. H.; Allendorf, M. D.; Melius, C. F. *J. Phys. Chem.* **1994**, *98*, 6995.
(19) Wloch, M.; Gour, J. R.; Piecuch, P. *J. Phys. Chem. A* **2007**, *111*, 11359.
(20) Piecuch, P.; Wloch, M. *J. Chem. Phys.* **2005**, *123*, 224105.
(21) Piecuch, P.; Wloch, M.; Gour, J. R.; Kinal, A. *Chem. Phys. Lett.* **2006**, *418*, 467.
(22) Ge, Y. B.; Gordon, M. S.; Piecuch, P. *J. Chem. Phys.* **2007**, *127*, 174106.
(23) Ge, Y. B.; Gordon, M. S.; Piecuch, P.; Wloch, M.; Gour, J. R. *J. Phys. Chem. A* **2008**, *112*, 11873.
(24) Steinfeld, J. I. Francisco, J. S. Hase, W. L. *Chemical Kinetics and Dynamics*; Prentice-Hall: Upper Saddle River, NJ, 1999.
(25) Corchado, J. C.; Chuang, Y.-Y.; Fast, P. L.; Hu, W.-P.; Liu, Y.-P.; Lynch, G. C.; Nguyen, K. A.; Jackels, C. F.; Ramos, A. F.; Ellingson, B. A.; Lynch, B. J.; Melissas, V. S.; Villa, J.; Rossi, I.; Coitino, E. L.; Pu, J.; Albu, T. V.; Garrett, B. C.; Isaacson, A. D.; Truhlar, D. G. POLYRATE 9.4.3: Computer Program for the Calculation of Chemical Reaction Rates for Polyatomics; 2006.
(26) Dean, A. M. *J. Phys. Chem.* **1985**, *89*, 4600.
(27) Hidaka, Y.; Shiba, S.; Takuma, H.; Suga, M. *Int. J. Chem. Kinet.* **1985**, *17*, 441.
(28) Curran, H. J. *Int. J. Chem. Kinet.* **2006**, *38*, 250.
(29) Michael, J. V.; Su, M. C.; Sutherland, J. W.; Harding, L. B.; Wagner, A. F. *Proc. Combust. Inst.* **2005**, *30*, 965.
(30) Sutherland, J. W.; Su, M. C.; Michael, J. V. *Int. J. Chem. Kin.* 2001, *33*, 669.
(31) Arutyunov, V. S.; Vedeneev, V. I.; Moshkina, R. I.; Ushakov, V. A. *Kinet. Catal.* **1991**, *32*, 234.
(32) Cobos, C. J.; Troe, J. *Z. Phys. Chem. Neue Folge* **1990**, *167*, 129.
(33) Lessing, P. A.; Heaps, R. J. *Nucl. Technol.* **1994**, *108*, 207.
(34) Hong, S. G.; Byun, T. S.; Lowden, R. A.; Snead, L. L.; Katoh, Y. *J. Am. Ceram. Soc.* **2007**, *90*, 184.

JP911673H